[19]If a term $h(S_{12}-S_0)^2/m_\pi{}^4$ is added to Eq. (13), the $E^*_{\pi 0}$ fits yield $h = 0.01 \pm 0.06$ with no change in g or in the χ^2.

[20]R. Messner, A. Franklin, R. Morse, U. Nauenberg, D. Dorfan, D. Hitlin, J. Liu, and R. Piccioni, in *Proceedings of the XVI International Conference on High Energy Physics, Chicago-Batavia, 1972,* edited by J. D. Jackson and A. Roberts (NAL, Batavia, Ill., 1973) Vol. 2, p. 209. These authors find that a quadratic term is necessary to fit the $E^*_{\pi 0}$ distribution.

PHYSICAL REVIEW D VOLUME 8, NUMBER 7 1 OCTOBER 1973

Search for Rare K^+ Decays. I. $K^+ \to \mu^+ \nu \bar{\nu} \nu$*†

C. Y. Pang and R. H. Hildebrand
Enrico Fermi Institute and Department of Physics, The University of Chicago, Chicago, Illinois 60637

G. D. Cable
Enrico Fermi Institute, The University of Chicago
and Department of Physics, The University of Arizona, Tucson, Arizona 85721

R. Stiening‡
Lawrence Berkeley Laboratory, Berkeley, California 94720

(Received 14 May 1973)

In a counter experiment at the LBL Bevatron, we have searched for the process $K^+ \to \mu^+ \nu \bar{\nu} \nu$ and have found no evidence for its existence. We have recorded ten events which could be examples of this decay mode, but could also be examples of $K^+ \to \mu^+ \nu \gamma$ in which the γ was not detected. Treating these as unidentified events and assuming the μ^+ spectrum proposed by Bardin, Bilenky, and Pontecorvo, we obtain a decay rate $\Gamma(K^+ \to \mu^+ \nu \bar{\nu} \nu) \leq 6 \times 10^{-6} \Gamma(K^+ \to \text{all})$ (90% confidence level). The data are presented in such a way as to allow calculation of rates for any assumed spectrum. The experiment provides a test for higher-order weak processes and sets constraints on certain first-order models.

I. INTRODUCTION

A. Experiments on Two K^+ Decay Modes

In this and a following paper we report on concurrent experiments to search for the K^+ decay modes $K^+ \to \mu^+ \nu \bar{\nu} \nu$ (I) and $K^+ \to \pi^+ \nu \bar{\nu}$ (II). Since the apparatus was common to the two experiments, its description in I will serve both papers.

B. The Decay $K^+ \to \mu^+ \nu \bar{\nu} \nu$

In an earlier publication[1] we have given preliminary results of a search for the decay process $K^+ \to \mu^+ \nu \bar{\nu} \nu$. We now present final results and give a detailed account of the work.

The well-known current-current theory of weak interactions appears to give an adequate description of all observed weak processes. This theory leads to divergences, however, when applied to certain high-order interactions, and at very high energies it leads to the violation of unitarity.[2]

The decay process

$$K^+ \to \mu^+ \nu \bar{\nu} \nu \qquad (1)$$

cannot occur in the first order of the conventional theory. The experimental investigation of this process may therefore give information about the structure of higher-order weak effects. Furthermore, since this decay process involves an extraordinary number of fermions, neutrinos in particular, its investigation provides information on two proposed first-order effects: (1) a neutrino-neutrino interaction other than the usual weak interaction (such an interaction could be very strong without having been seen[3]), and (2) a six-fermion interaction[4,5] in addition to the ordinary (four-fermion) weak interaction.

For K's decaying at rest, process (1) should be uniquely distinguished from all known decays by the emission of μ's in the energy interval $60 < T_\mu < 100$ MeV unaccompanied by other charged particles or by γ's. In this experiment, K's from the LBL Bevatron were brought to rest in a carbon stopper. The K's and their decay products were detected by an array of scintillation and Čerenkov counters. The μ's were identified by their μ-e decays; the μ energies were determined by range. In order to reject background events from pro-

cesses such as $K^+ \to \mu^+ \pi^0 \nu$ and $K^+ \to \mu^+ \nu \gamma$, the whole decay region was surrounded by a high-efficiency γ detector composed of Pb-glass Čerenkov radiators.

II. THEORY

A. Conventional Weak-Interaction Theory

All observed weak processes can be described phenomenologically by the effective Lagrangian

$$L_{\mathrm{wk}} = \frac{G}{\sqrt{2}} J_\lambda^\dagger J_\lambda ,$$

where $G \simeq 10^{-5}/m_p^2$ is the Fermi coupling constant (m_p = proton mass), and $J_\lambda = J_\lambda^h + J_\lambda^l$ is the weak current. The leptonic component of J_λ is given by

$$J_\lambda^l = \bar{e}\gamma_\lambda(1+\gamma_5)\nu_e + \bar{\mu}\gamma_\lambda(1+\gamma_5)\nu_\mu ,$$

and the hadronic component has the form

$$J_\lambda^h = V_\lambda - A_\lambda ,$$

with V_λ a polar and A_λ an axial-vector current operator.

Because of the four particles in the final state, process (1) cannot occur in the first order of this theory. It can, however, occur as the result of second-order interactions. For the two "tree" diagrams shown in Fig. 1, the rate can be calculated as in the Appendix. Since there are two vertices in each of these diagrams, the corresponding rates are suppressed by a factor $G^2 m_K^4$ with respect to the process $K^+ \to \mu^+ \nu$. For the energy interval $60 < T_\mu < 100$ MeV observed in the experiment, the rate $\Gamma(K^+ \to \mu^+ \nu \bar{\nu} \nu)$ is calculated to be $3.7 \times 10^{-16}\, \Gamma(K^+ \to \mu^+ \nu)$, which is far below the rate observable in this experiment.

These diagrams, however, are not the only ones which could contribute to the decay. There are, in addition, "loop" diagrams for which divergences appear. Hence it is not possible with existing theoretical techniques to make a rigorous calculation of the rate. In view of this difficulty and the absence of any previous sensitive tests of higher-order weak effects, it has appeared valuable to make an experimental investigation.

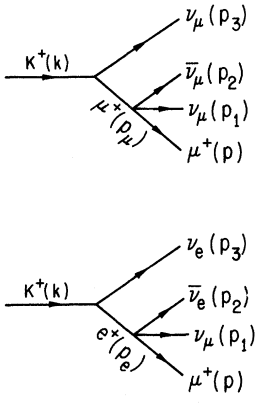

FIG. 1. Second-order diagrams for the process $K^+ \to \mu^+ \nu \bar{\nu} \nu$.

B. First-Order Models

1. *Neutrino-Neutrino Interaction*

Bardin, Bilenky, and Pontecorvo,[3] and Bialynicki-Birula[6] have raised the possibility of a ν-ν interaction other than the weak interaction. They have pointed out that such an interaction could be much stronger than the weak interaction without being evident in existing experimental data.

Bardin *et al.*[3] assume an interaction between neutrinos of the form

$$H_{\nu\nu} = F(\bar{\nu}\gamma_\lambda \nu)(\bar{\nu}\gamma_\lambda \nu) ,$$

where F is the hypothetical ν-ν interaction constant. Using the pole approximation to calculate the differential decay rate for process (1) (see Fig. 2) they obtain the expression

$$\frac{d\Gamma}{dx} = \frac{1}{2^7 \pi^5} G^2 F^2 f_K^2 m_K (1 + r^2 - 2x)(x^2 - r^2)^{1/2} \times [(1-2x)x + r^2] , \quad (2)$$

where $r = m_\mu/m_K$, $x = E_\mu/m_K$, and E_μ is the total energy of the muon. The corresponding total decay rate is

$$\Gamma(K^+ \to \mu^+ \nu \bar{\nu} \nu) = \frac{1}{15\pi^5 2^{11}} G^2 F^2 f_K^2 m_K^7 .$$

Comparing this to the $K^+ \to \mu^+ \nu$ decay rate, we obtain

$$\frac{\Gamma(K^+ \to \mu^+ \nu \bar{\nu} \nu)}{\Gamma(K^+ \to \mu^+ \nu)} = 0.51 \times 10^{-5} F^2 m_p^4 .$$

From our measurement of this ratio we are able to set a limit

$$\left|\frac{F}{G}\right| < 1.7 \times 10^5 \text{ (90\% confidence level)}.$$

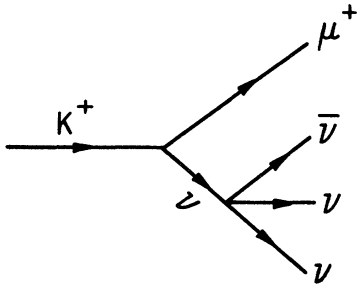

FIG. 2. Diagram for $K^+ \to \mu^+ \nu \bar{\nu} \nu$ involving a neutrino-neutrino interaction.

2. *Six-Fermion Interaction*

The notion of a six-fermion interaction was first put forward to explain an inaccurate experimental report of a $\Delta S = -\Delta Q$ process. Although subsequent tests have given no positive evidence for $\Delta S = -\Delta Q$ processes, there has been continuing interest in the possibility that six-fermion interactions exist in nature. If they do exist, they should become increasingly evident with increasing energy.

Ericson and Glashow[4] have pointed out that processes such as

$$\nu p \to \nu p \mu^+ e^-,$$
$$\to \nu p \mu^+ \mu^- ,$$
$$\mu p \to \nu p \bar{\nu} e ,$$

could occur through the interaction Hamiltonian

$$H = \frac{G}{\sqrt{2}} \frac{1}{\lambda^3} (\bar{p}p) J_\lambda^l J_\lambda^{l\dagger} ,$$

where λ is a parameter which characterizes the strength of the six-fermion coupling. A limit $\lambda > 100$ MeV is indicated by inelastic ν-p scattering experiments.[7]

Recently, Vanzha, Isaev, and Lapidus[5] have extended the idea of six-fermion interaction to the possible decay of mesons into four leptons. They construct the six-fermion interaction in close analogy with the four-fermion interaction. For process (1) they choose an effective matrix element in the form

$$M = i f_K \Phi k_\alpha \{ F_1 [\bar{\mu}(1+\gamma_5)\nu_\mu][\bar{\nu}_e \gamma_\alpha (1+\gamma_5)\nu_e] + F_2 [\bar{\mu}\sigma_{\alpha\beta}(1+\gamma_5)\nu_\mu][\bar{\nu}_e \gamma_\beta (1+\gamma_5)\nu_e] \} + i f_K \Phi m_K F_3 [\bar{\mu}\gamma_\alpha (1+\gamma_5)\nu_\mu][\bar{\nu}_e \gamma_\alpha (1+\gamma_5)\nu_e] ,$$

where Φ is the wave function of the K meson and k_α is its four-momentum. The theoretical estimate of this process is complicated in such a model by the appearance of the unknown form factors F_i $(i = 1, 2, 3)$. However, simply assuming that all form factors are equal and constant in the matrix element, they evaluate the differential and the total decay rates,

$$\frac{d\Gamma}{dE_\mu} = f_K^2 F_s^2 2^9 R \left(1 + \frac{m_\mu}{E_\mu}\right) ,$$

and

$$\Gamma(K^+ \to \mu^+ \nu \bar{\nu} \nu) = \frac{f_K^2 m_K}{5\pi^2 6^4} (p_\mu^{\max})^8 \, 18.6 F_s^2 ,$$

where

$$R = \frac{m_K p_\mu A^2 E_\mu}{3\pi^5 2^{13}} (2p_\mu^3 + 4p_\mu^3 A + \tfrac{5}{2} p_\mu A^2 + \tfrac{1}{2} A^3) ,$$

$$A = m_K - E_\mu - p_\mu ,$$

$$p_\mu^{\max} = \frac{(m_K^2 - m_\mu^2)}{2m_K} ,$$

and F_s is the common form factor which can be related to the usual four-fermion interaction constant G by the expression

$$F_s = \frac{G}{\sqrt{2}} \frac{1}{\lambda^3} .$$

The constant λ is an unknown parameter with the dimensions of mass. If the $K^+ \to \mu^+ \nu \bar{\nu} \nu$ decay is indeed due to the presence of a six-fermion interaction, we derive the expression[8]

$$\frac{\Gamma(K^+ \to \mu^+ \nu \bar{\nu} \nu)}{\Gamma(K^+ \to \mu^+ \nu)} = 0.3 \left(\frac{m_\mu}{\lambda}\right)^6 . \tag{3}$$

Our measurement of this ratio yields the limit

$$\lambda > 677 \text{ MeV} \quad (90\% \text{ confidence level}).$$

C. Other Models

The models we have discussed are not the only ones which could lead to the occurrence of $K^+ \to \mu^+ \nu \bar{\nu} \nu$. In Sec. V B3 we give a procedure for calculating constraints on any model which yields a well-specified μ^+ spectrum.

III. PREVIOUS RESULTS

There has been no earlier experiment to search directly for $K^+ \to \mu^+ \nu \bar{\nu} \nu$. But we can infer a limit for the related process $K^+ \to e^+ \nu \bar{\nu} \nu$ from experiments on $K^+ \to e^+ \nu$. The positron spectrum observed by Heard *et al.*[9] contains "background" events above the maximum for $K^+ \to e^+ \pi^0 \nu$ (228 MeV/c) and below the peak for $K^+ \to e^+ \nu$ (247 MeV/c). If we assume that all the (111) events in the interval 230–240 MeV/c are possible examples of $K^+ \to e^+ \nu \bar{\nu} \nu$, and assume a decay spectrum for this process based on the model of Bardin *et al.*[3] [Eq. (2)] ($\approx$1% of the spectrum between 230 and 240 MeV/c), we obtain a limit on the $K^+ e^+ \nu \bar{\nu} \nu$ branching ratio of 8.5×10^{-5} and a limit $F < 1.3 \times 10^6 G$. This limit on F is lower than that which can be inferred from existing neutrino scattering experiments.[10] The corresponding limit on process (1) would be $\Gamma(K^+ \to \mu^+ \nu \bar{\nu} \nu) < 5.5 \times 10^{-4} \, \Gamma(K^+ \to \text{all})$.

IV. EXPERIMENT

As stated in the Introduction, our discussion here of the experimental procedure will serve both for $K^+ \to \mu^+ \nu \bar{\nu} \nu$ (I) and for $K^+ \to \pi^+ \nu \bar{\nu}$ (II). In most respects the two experiments were identical; they used the same apparatus, the same calibrations, and very nearly the same techniques for event selection and analysis.

A. Distinguishing Characteristics of the Decays $K^+ \to \mu^+\nu\bar{\nu}\nu$ and $K^+ \to \pi^+\nu\bar{\nu}$

The known decays of the K^+ meson are listed in Table I. The range distributions including straggling and multiple scattering for decays yielding π^+ and μ^+ are shown in Fig. 3.

The process $K^+ \to \mu^+ \nu \bar{\nu} \nu$ ($K^+ \to \pi^+ \nu \bar{\nu}$) is distinguished from all known decay modes by the emission of a single μ^+ (π^+) without emission of other charged particles and without emission of γ rays. The emitted μ^+ (π^+) is further distinguished in having a kinematically allowed spectrum extending through all energies up to 152.6 MeV (127 MeV) [all $\mu^+(\pi^+)$ ranges in carbon up to 62.5 g/cm^2 (43.5 g/cm^2)].

On the basis of these characteristics we established the following experimental requirements for identification of $K^+ \to \mu^+ \nu \bar{\nu} \nu$ ($K^+ \to \pi^+ \nu \bar{\nu}$) events:

(i) The K^+ must decay at rest within a well-defined region, the carbon stopper.

(ii) The decay of the K^+ must produce a single charged particle. We exclude events in which additional charged particles emerge from the stopper.

(iii) The charged particle must be identified as a $\mu^+(\pi^+)$ by observing the $\mu^+ \to e^+$ ($\pi^+ \to \mu^+ \to e^+$) decay signal. In the case of $\pi^+ \to \mu^+ \to e^+$ decays the μ^+ must have the energy expected for $\pi^+ \to \mu^+ \nu$ (4 MeV).

(iv) The μ^+ range must be greater than the range of μ's from decay-in-flight of π^+ following $K^+ \to \pi^+\pi^0\pi^0$ or $K^+ \to \pi^+\pi^+\pi^-$, and less than the range of π's from $K^+ \to \pi^+\pi^0$. (The π^+ range must be greater than the maximum for $K^+ \to \pi^+\pi^+\pi^-$ or $K^+ \to \pi^+\pi^0\pi^0$ and less than the range for $K^+ \to \pi^+\pi^0$.)

(v) The emission of γ's in any direction must be excluded.

With suitable changes in these requirements it was possible to select samples of the decay modes $K^+ \to \pi^+\pi^0$, $K^+ \to \mu^+\nu$, and $K^+ \to \mu^+\pi^0\nu$ for calibration.

TABLE I. The known decay modes of the K^+ and ranges of the decay π's and μ's.

Decay mode	Branching ratio [a]	Range (g/cm^2 in carbon)
$K^+ \to \mu^+\nu$	$(63.77 \pm 0.28) \times 10^{-2}$	$R_\mu = 62.2$
$K^+ \to \pi^+\pi^0$	$(20.92 \pm 0.29) \times 10^{-2}$	$R_\pi = 34.6$
$K^+ \to \mu^+\pi^0\nu$	$(3.20 \pm 0.11) \times 10^{-2}$	$R_\mu \leq 52.3$
$K^+ \to \pi^+\pi^+\pi^-$	$(5.58 \pm 0.03) \times 10^{-2}$	$R_\pi \leq 9.7$
$K^+ \to \pi^+\pi^0\pi^0$	$(1.68 \pm 0.04) \times 10^{-2}$	$R_\pi \leq 11.4$
$K^+ \to e^+\pi^0\nu$	$(4.86 \pm 0.07) \times 10^{-2}$	
$K^+ \to e^+\pi^0\pi^0\nu$	$(1.8^{+2.4}_{-0.6}) \times 10^{-5}$	
$K^+ \to \pi^+\pi^-e^+\nu$	$(3.7 \pm 0.2) \times 10^{-5}$	$R_\pi \leq 38.4$
$K^+ \to \pi^+\pi^0\mu^+\nu$	$(0.9 \pm 0.4) \times 10^{-5}$	$R_\pi \leq 12.2$, $R_\mu \leq 22.2$
$K^+ \to e^+\nu$	$(1.60 \pm 0.12) \times 10^{-5}$ [b]	
$K^+ \to \mu^+\nu\gamma$	$(4.1) \times 10^{-3}$ [c]	$R_\mu \leq 62.2$
$K^+ \to \pi^+\pi^0\gamma$	$(2.55 \pm 0.18) \times 10^{-4}$ [d]	$R_\pi \leq 34.6$
$K^+ \to e^+\pi^0\nu\gamma$	$(3.7 \pm 1.4) \times 10^{-3}$ [e]	
$K^+ \to \pi^+\pi^+\pi^-\gamma$	$(1.0 \pm 0.4) \times 10^{-4}$ [f]	$R_\pi \leq 9.7$

[a] From Ref. 13 except as noted.
[b] Reference 10.
[c] Calculated from inner bremsstrahlung, Ref. 16, $E_\gamma > 10$ MeV.
[d] $T_{\pi^+} = (55-90$ MeV), Ref. 17.
[e] $E_\gamma > 10$ MeV.
[f] $E_\gamma > 11$ MeV.

B. Experimental System

The experimental system designed to meet the above requirements is shown in Figs. 4–10. The principal components of the system are:

(1) the beam channel—produces a partially separated momentum-analyzed beam of K^+'s,

(2) the K telescope (Fig. 6)—slows and identifies K's, stops protons, and rejects π's, μ's, e's, and γ's,

(3) the stopper assembly (Fig. 7)—stops K's, defines the decay region, and rejects events with multiple charged particles,

(4) the decay telescope (Figs. 8 and 9)—identifies and measures the range of K-decay secondaries, (a) the defining counters (T1–T4, TS)—define the telescope geometry and select stopping pions and muons, (b) the degrader—slows the secondaries and selects the range interval, (c) the

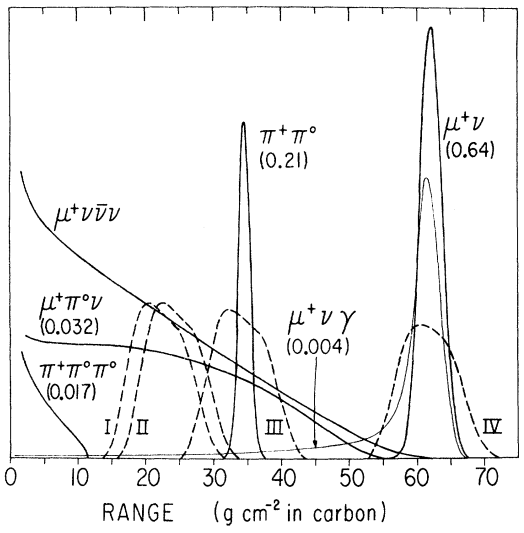

FIG. 3. Range spectra for decays of the type $K^+ \to (\pi^+$ or $\mu^+) +$ neutrals, with straggling and multiple scattering taken into account. Vertical scales are arbitrary. Branching ratios are shown in brackets (the value for $\mu^+\nu\gamma$ corresponds to a cutoff $E_\gamma > 10$ MeV). Curve for $K^+ \to \mu^+\nu\bar{\nu}\nu$ corresponds to momentum spectrum given by Bardin *et al.* (Ref. 3). Dashed curves show geometric detector efficiencies versus range for degrader thickness used to detect $K^+ \to \mu^+\pi^0\nu$ and $K^+ \to \mu^+\nu\bar{\nu}\nu$ [(I) and (II)], $K^+ \to \pi^+\pi^0$ (III), and $K^+ \to \mu^+\nu$ (IV).

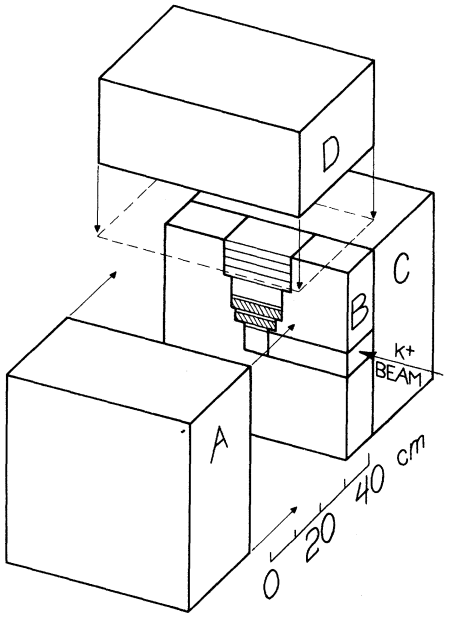

FIG. 4. Apparatus: Arrangement of main components. A, C, and D are Čerenkov radiators; B is assembly of radiators, scintillators, and degraders (see Fig. 5). A, B, C, and D are adjacent during operation. Access to B is provided by displacing A as shown. D is raised in figure to show section B.

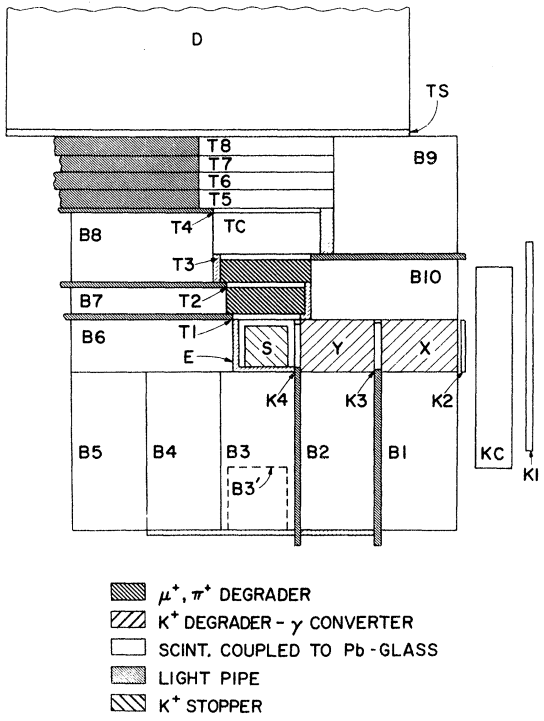

FIG. 5. Apparatus: Central section (section B of Fig. 4). Outputs of T5–T8 are displayed on oscilloscopes. The oscilloscope traces are scanned for π-μ-e or μ-e decays. γ's (e.g., from $K^+ \to \mu^+\pi^0\nu$, $\mu^+\nu\gamma$) are vetoed by lead-glass Čerenkov detectors A, B1–B10, C, and D. (Each block is separately viewed except TC and B7–B10, which are coupled to A and C.) B3 is replaced by a smaller block B3′ (dashed line) for single γ-efficiency check (see text). X and Y are "sandwich blocks" to slow K's and convert outgoing γ's (see Fig. 6).

decay counters (T5–T8)—stop secondaries in the selected range interval and detect μ-e and π-μ-e decays,

(5) the γ detector (blocks A, B1–B10, C, D, X, and Y—see Figs. 4, 5, and 6)—detects γ's moving in any direction,

(6) the triggering logic (Fig. 10)—selects events to be recorded,

(7) the display system—displays and records information on each event (see sample-event Fig. 11), and

(8) the iron box—provides light shielding and magnetic shielding.

As we discuss these components it will be evident that the configuration of the apparatus is largely determined by the array of lead-glass blocks which serve as converters and Čerenkov radiators for detection of γ's emerging from the stopper.

1. *Beam Channel*

The K^+ beam was produced in a platinum target (0.5 in. × 0.2 in. × 2.0 in.) in the external 6.2 GeV/c proton beam of the LBL Bevatron. The momentum of the beam was defined by a bending magnet and collimator to be 510 MeV/c. The beam was transported through a crossed-field separator, and focused on the carbon stopper. The beam cross section at the stopper was about 3×3 cm^2. With a beam intensity of 10^{12} protons/pulse,

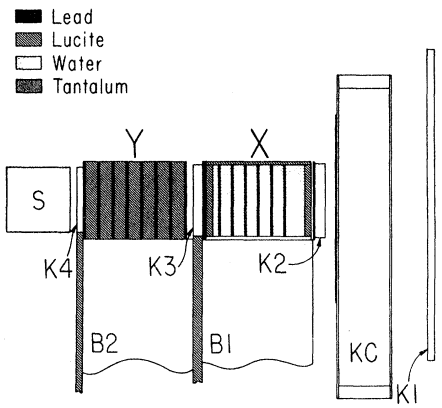

FIG. 6. K telescope: Counters K1–K4 detect incoming beam particles. Pions are vetoed by water Čerenkov detector KC. Sandwiches of tantalum and water (X) and lead and lucite (Y), optically coupled to lead-glass blocks B1 and B2, slow incoming K's and convert and detect outgoing γ's. K's come to rest in stopper S.

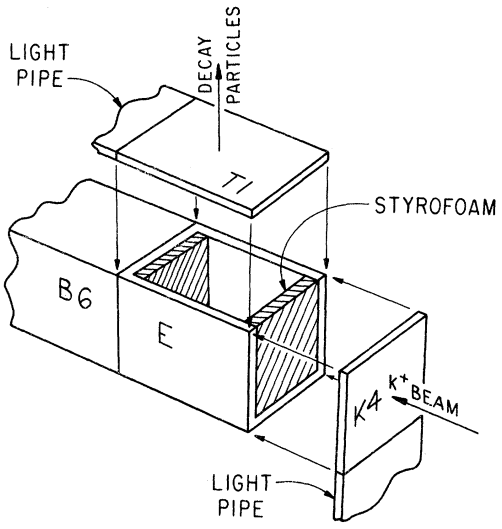

FIG. 7. K^+ stopper assembly: The stopper (carbon granules, 0.79 g/cm^3) fills the interior of scintillator box E. Styrofoam spacers set the length of the stopper along the K^+ beam direction (5 g/cm^2). The stopper is completely surrounded by scintillator E (optically coupled to lead-glass block B6) and counters K4 and T1. K4 and T1 are displaced in the figure to show the configuration of the box.

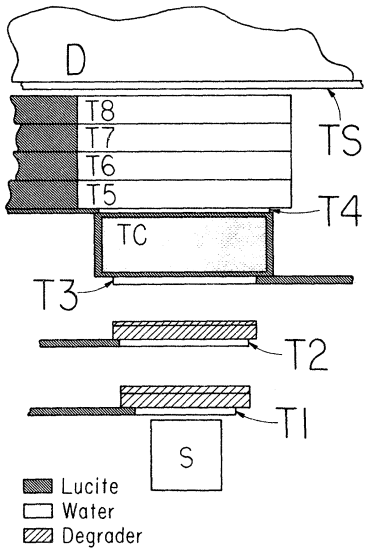

FIG. 8. Decay telescope: The defining counters T1–T4, TS (optically coupled to lead-glass block D), T9, and T10 (shown in Fig. 9) select decays in which a charged particle stops in the decay counters T5–T8. The water box TC discriminates against electrons and fast muons. Carbon plates between counters T1 and T3 select the range interval of the decay counters. The degrader configuration shown corresponds to curve II of Fig. 3.

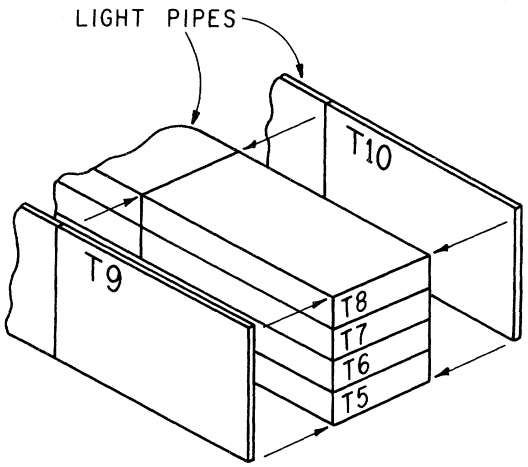

FIG. 9. Placement of the side counters T9 and T10: The counters are used to detect particles escaping from the sides of T5–T8. They are adjacent during operation. The signal from the side counters is displayed on a scope trace, and, as part of the D signal, used in the triggering logic. Data taken with the T9, T10 anticoincidence requirement removed were used to calculate the correction for particles emerging from the ends of the decay counters.

about 5000 K^+/pulse came to rest in the carbon stopper. At our apparatus, the K/π ratio was $\sim\frac{1}{20}$.

2. *K Telescope*

The K telescope consisted of scintillation counters K1 to K4, water Čerenkov detector KC, and two "sandwich blocks" X and Y (see Fig. 6). The large scintillation counter K1 detected all charged particles entering the apparatus and aided in identifying background events due to scattered beam particles (see Sec. IV C). Counters K2 to K4 selected particles which entered the decay region and discriminated against π's and lighter particles on the basis of energy loss. [At K3, $(dE/dx)_K > 1.5(dE/dx)_\pi$]. The water Čerenkov counter KC, in anticoincidence, was triggered by π's, μ's, and e's but not by K's.

The "sandwich blocks" X and Y consisted of layers of tantalum and water (X), and lead and lucite (Y). These blocks served as degraders to slow the beam particles, and as converters and Čerenkov radiators (4.3 radiation lengths, total) to detect outgoing γ's (i.e., the blocks served as part of the γ detector surrounding the stopper). Water and lucite were chosen to give Čerenkov thresholds just above the K velocities at X and Y. The blocks were of such a thickness that all protons stopped before reaching K4, most K's stopped within the stopper, and nearly all π's, μ's, and e's went beyond the stopper and through scintillator E attached to B6.

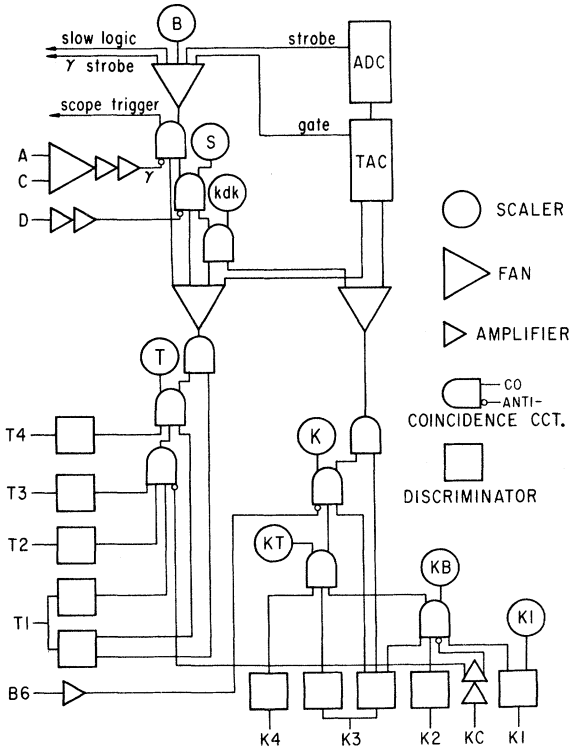

FIG. 10. Triggering logic: K's stopping in the stopper are selected by the signal K1, $\overline{KC}$, K2, K3 [pulse height $> 1.5 \times$ (pion pulse height)], K4, $\overline{B6}$. Decay particles stopping in the decay counters T5–T8 are indicated by T1, T2, T3, $\overline{TC}$, T4, $\overline{D}$, where T1 is > 3 ns after K3. Signals from lead-glass blocks A and C form the γ anticoincidence signal. The ADC output is displayed on data lights for recording with the oscilloscope traces. All counters shown except KC, B6, A, and C supply signals to the oscilloscopes (see Fig. 11) as well as to the triggering logic. Scalers are used to monitor the operation of the apparatus.

3. *Stopper Assembly*

The K's came to rest and decayed within a stopper S (Fig. 5) composed of carbon granules (mean density 0.79 g/cm^3). The granules were contained in a box, made of plastic scintillators, with inside cross section 6.4×6.4 cm^2 and inside length (within Styrofoam spacers) 6.3 cm or 5.0 g/cm^2 (Fig. 7). The dimensions and density of the stopper were large enough so that most of the K's stopped in the carbon, but small enough so that nearly all decay particles reached the surrounding counters. The triggering system (see below) selected events in which a beam particle passed through K4 without reaching E and in which after a delay, a decay particle was detected in T1.

4. *Decay Telescope*

Counters T1 to T4 (Fig. 8) selected events in which a charged particle from the stopper entered the decay counters T5 to T8. Scintillator TS (above T8 and optically coupled to lead-glass block D) ensured that the K-decay particle did not pass completely through the decay counters. Additional discrimination against electrons and fast muons was provided by a water Čerenkov box TC between counters T3 and T4. The water box was optically coupled to lead-glass blocks A and C and its output was observed as part of the γ detector signal. Counters T9 and T10 (Fig. 9) used in the last two-thirds of the experiment ensured that the particle did not go out the sides of the decay counters. In particular they prevented π-μ-e decays from simulating μ-e decays when the π and e passed through the decay counters and the π-μ decay occurred outside.

Degrading material between counters T1 and T3 slowed the K-decay secondaries and defined the range interval covered by the decay counters. Carbon was used for the degrader material wherever possible to minimize absorption of pions. Because of space limitations, copper was used for the $K^+ \to \mu^+ \nu$ calibration.

Muons and pions in the range interval under investigation stopped in the four $2.5 \times 10.2 \times 19.1$ cm^3 decay scintillators T5 to T8. A rough determination of the range within the interval set by the degrader was given by the location of the counter in which the particle stopped. The particles were identified by the $\mu \to e$ and $\pi \to \mu \to e$ decay signals appearing in T5 to T8.

In the course of the experiment, four different degrader configurations were used. One, chosen primarily for $K^+ \to \mu^+ \nu \bar{\nu} \nu$ was sufficient to stop muons from the decay-in-flight of pions from $K^+ \to \pi^+ \pi^+ \pi^-$ before they reached the decay counters. (Fig. 8 illustrates this degrader.) Another, chosen primarily for $K^+ \to \pi^+ \nu \bar{\nu}$, set the lower limit of the decay-counter range interval slightly above the $K^+ \to \pi^+ \pi^+ \pi^-$ end point. In both cases, π^+'s from $K^+ \to \pi^+ \pi^0$ went beyond T8 and were vetoed by TS. Two other degrader configurations were used for calibrations with $K^+ \to \pi^+ \pi^0$ and $K^+ \to \mu^+ \nu$. The four degraders and their corresponding decay-counter range intervals are summarized in Table II.

5. *γ Detector*

The distinctive technical feature of the experiment was the Pb-glass Čerenkov counter array surrounding the stopper. This array, with a thickness of about 10 radiation lengths, detected γ's (e.g., γ's from $K^+ \to \mu^+ \nu\gamma$ or from $K^+ \to \pi^+ \pi^0$, $\mu^+ \pi^0 \nu$; $\pi^0 \to \gamma\gamma$) emitted from the stopper. γ-rays going through the entrance channel were detected by the X and Y radiators as described above. Each of the Pb-glass blocks B1-B6 (Fig. 5) was viewed

TABLE II. Degrader configurations used in this experiment. Degrader numbers correspond to efficiency curves shown in Fig. 3. The half-thickness of the stopper (stopper center to T1) is 2.73 g/cm^2. The total amount of material other than the degrader between the stopper and T5 is 10.08 g/cm^2. The decay counters T5–T8 are each 2.84 g/cm^2 thick (total, including counter wrapping, 11.58 g/cm^2).

Degrader	Thickness (g/cm^2 in carbon)	Detection range interval (g/cm^2 in carbon)
I	2.80	12.9–31.2
II	6.16	16.3–34.8
III	15.72	25.9–45.0
IV	42.61	52.7–73.7

by a 56DVP phototube. Blocks B1 and B2 were optically isolated from the others and used to view pulses due to γ's converted in the entrance channel. Blocks B7–B10 were optically coupled to blocks A and C. A and C were each viewed by one 56DVP and four 60AVP phototubes. Block D was optically decoupled from the others and was viewed by two 60AVP phototubes.

Calibration of the γ detector, as described in Sec. IV D, indicated an inefficiency $I_{\pi^0} < 2.2 \times 10^{-5}$ (90% confidence level) for π^0's, and an average inefficiency $I_\gamma = 0.013$ for single γ's of 20 to 50 MeV.

6. *Triggering Logic*

The triggering logic (Fig. 10) selected events for which (i) a K^+ stopped in the stopper (the signal K), (ii) a decay particle entered the decay telescope (the signal T), (iii) the decay particle appeared later than the K^+ and stopped before reaching TS (the signal S), and (iv) no γ's were emitted (the signal $\overline{\gamma}$). In terms of counter pulses these signals were defined as follows:

$$K = \text{K1, K2, K3, K4, } \overline{\text{KC}}, \overline{\text{B6}}\,(\overline{\text{E}}) ,$$

where the bar denotes anticoincidence (K2, K3, and K4 pulse discriminators set to accept K's and reject π's as discussed in Sec. IV B2),

$$T = \text{T1, T2, T3, T4} ,$$

$$S = \text{K, T, } \overline{\text{D}}\ (\overline{\text{TS}}, \overline{\text{T9}}, \overline{\text{T10}}) ,$$

where a delay > 3.3 ns was required between K and T, and

$$\gamma = \text{A, C} ,$$

where blocks B7–B10 and TC were optically coupled to A and C.

The signals from the phototubes on B1–B6 were not included in the triggering logic but were displayed on counter lights or oscilloscope traces. The $\overline{\gamma}$ triggering level was set to obtain a convenient picture-taking rate, not to eliminate all events accompanied by γ's.

The trigger S was used for $K^+ \to \pi^+\pi^0$, $\mu^+\pi^0\nu$, and $\mu^+\nu$ events; the trigger $S\overline{\gamma}$ for $K^+ \to \mu^+\nu\overline{\nu}\nu$ and $\pi^+\nu\overline{\nu}$.

7. *Display System*

The information on each event accepted by the triggering logic was displayed on four 4-beam oscilloscopes and an array of counter lights as shown in Fig. 11.

The event in the figure is a $K^+ \to \pi^+\pi^0$ decay. The traces K1–4 and T1–4 indicate that a single particle passed through each counter. Since traces B1 and B2 are undeflected except for timing pulses, we conclude that no γ was converted in the radiators X and Y of the K channel. Inset (A) of Fig. 11 shows how these traces looked when a γ did convert in the K channel. The γ lights indicate γ detection in blocks A, B3, and C. Each phototube on blocks A and C is separately displayed.

The fast scope traces (15 ns/cm) show that a π stopped in counter T5, and decayed to a μ in a little over one mean life. The μ pulse height corresponds to the expected energy, 4.1 MeV. The slow scope traces (0.4 μs/cm) show again the π and μ pulses (unresolved on this oscilloscope) and the pulses made after ~2 muon mean lives by the decay electron as it went out through T5–T8, T9 or T10, and TS. The K-life lights indicate a kaon lifetime of 32 ns.

8. *Iron Box*

The entire apparatus was enclosed in an iron box which provided light shielding and magnetic shielding. The apparatus was mounted on wheels so that it could be withdrawn from the box for service.

C. Scanning Criteria

Films recording the oscilloscope traces and phototube counter lights, as in Fig. 11, were displayed on a pair of Recordak film viewers. All accepted events met the following criteria: (i) Only one pulse was observed from each of the counters K1, K2, K3, K4, T1, T2, T3, and T4; (ii) on the slow scope no K1 pulse appeared in coincidence with the e pulse. (This excluded the simulation of decay electrons by scattered beam particles); and (iii) the e pulse (and for stopping π's, also the μ pulse) originated in the counter showing the stopping μ (or π).

D. Detection Efficiency

In determining the ratios $\Gamma(K^+ \to \mu^+\nu\overline{\nu}\nu)/\Gamma(K^+ \to \mu^+\nu)$ and $\Gamma(K^+ \to \pi^+\nu\overline{\nu})/\Gamma(K^+ \to \pi^+\pi^0)$ many efficiency factors including solid angle, π^+ absorption, π-μ

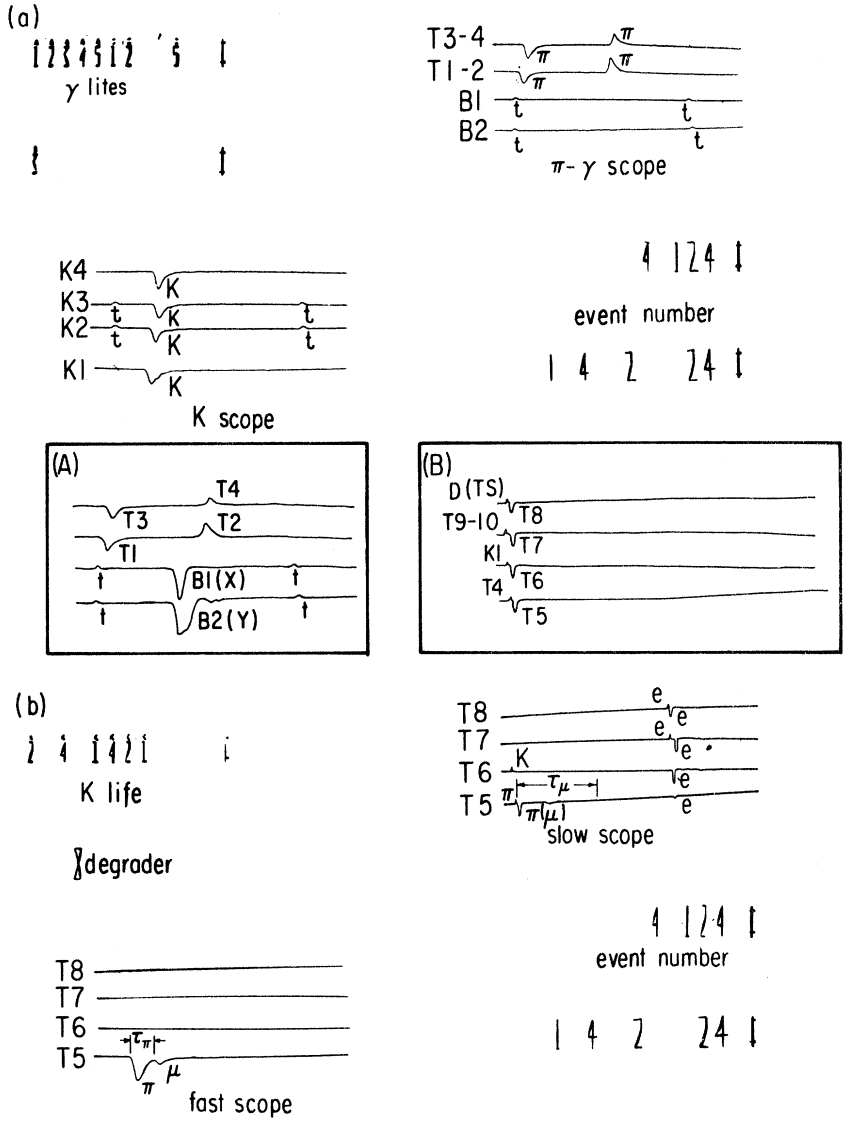

FIG. 11. A $\pi^+ \to \mu^+ \to e^+$ event from $K^+ \to \pi^+ \pi^0$: (a) view I, (b) view II. The oscilloscope traces are identified by the corresponding counter numbers. The pulses are labeled by the corresponding particles. Pulses labeled t are timing pulses (separation 200 ns). Distances corresponding to pion and muon mean lives are shown on the view II scopes. Inset A shows the appearance of the π-γ scope for an event in which a π^0 gamma is detected in the sandwich blocks X and Y. Inset B shows the format for coincident pulses in counters T4–T10, TS, and K1 as displayed on the slow oscilloscope.

pulse resolution, and chance coincidence corrections, canceled out in whole or in part. But since we wished to compare calibrations involving decays into both μ's and π's, it was necessary to consider all these factors.

1. *Efficiency vs Range*

The efficiency with which K-decay particles were stopped in the decay counters T5–T8 was calculated as a geometric quantity, taking into account the variation in solid angle as a function of the particle range for a given degrader thickness. This geometrical efficiency E was then folded with the decay spectrum for a particular decay mode to give the effective detection efficiency ϵ. Figure 3 shows the geometrical detector efficiencies versus range for each degrader. Table III gives effective detection efficiencies.

2. *Pion Transmission and Resolution*

For comparison of the calibrations using $K^+ \to \mu^+ \nu$ and $K^+ \to \pi^+ \pi^0$ it was necessary to know the fraction T of pions transmitted through the degrader, and the fraction C_π of $\pi \to \mu$ decays which could be re-

TABLE III. Effective detection efficiency for various decay modes and degraders I, II, III, and IV.

Decay mode	Effective detection efficiency
$K^+ \to \mu^+ \nu$	$\epsilon(\text{IV}) = 1.84 \times 10^{-2}$
$K^+ \to \pi^+ \pi^0$	$\epsilon(\text{III}) = 2.05 \times 10^{-2}$
$K^+ \to \mu^+ \pi^0 \nu$	$\epsilon(\text{I}) = 0.58 \times 10^{-2}$
	$\epsilon(\text{II}) = 0.52 \times 10^{-2}$
$K^+ \to \mu^+ \nu \gamma$	$\epsilon(\text{I}) = 0.41 \times 10^{-3}$
	$\epsilon(\text{II}) = 0.47 \times 10^{-3}$

solved on the fast oscilloscope traces. For measurement of the ratio $\Gamma(K^+ \to \pi^+ \nu \bar{\nu})/\Gamma(K^+ \pi^+ \pi^0)$ it was necessary only to know the ratio $T_{\pi^+ \pi^0}/T_{\pi^+ \nu \bar{\nu}}$ of the transmissions through the corresponding degraders.

The values $T_{\pi^+ \pi^0} = 0.70$ and $T_{\pi^+ \pi^0}/T_{\pi^+ \nu \bar{\nu}} = 0.81$ were calculated using measured values for the π^+-N inelastic cross sections.[11]

The factor $C_\pi = 0.66$ was determined empirically from the π^+ lifetime distribution for $K^+ \to \pi^+ \pi^0$ events (Fig. 12). This value corresponds to resolution of events with lifetime $> 0.41\ \tau_\pi$.

We are able to check these values of T and C_π by our calibrations as discussed below.

3. *Chance Coincidence of γ's*

In analyzing data taken with the $S\bar{\gamma}$ trigger (see Sec. IV B6 above) it was necessary to allow for valid events vetoed by γ's not associated with the observed K decay (e.g., γ's due to charge exchange of beam π^+'s followed by π^0 decay).

To determine this correction, we examined the $K^+ \to \mu^+ \nu$ calibration data for events in which there appeared to be associated γ's. The correction factor R is given by $R = (\text{Total number of } K^+ \to \mu^+ \nu \text{ events})/(K^+ \to \mu^+ \nu \text{ events without } \gamma \text{ signals})$. The value of R [R(average) = 1.48] was determined as a function of beam intensity and was checked at many times during the run.

4. *γ Inefficiency*

The efficiency of the γ detector for π^0's was determined by adjusting the degrader for detection of $K^+ \to \pi^+ \pi^0$ (degrader III, Fig. 3) and recording the γ signals in coincidence with π's stopping in the decay counters (with observed $\pi \to \mu \to e$ signals). Among 1.65×10^5 stopping π^+ we observed no event without a signal from at least one of the phototubes viewing the Pb-glass blocks. After correcting for chance coincidences we conclude that the probability of missing a π^0 from $K^+ \to \pi^+ \pi^0$ decay was $< 2.2 \times 10^{-5}$ (90% confidence level). This inefficiency was low enough to preclude background muons from $K^+ \to \mu^+ \pi^0 \nu$ or from the decay-in-flight of π^+ from $K^+ \to \pi^+ \pi^0 \pi^0$.

The efficiency of the γ detector for single γ's

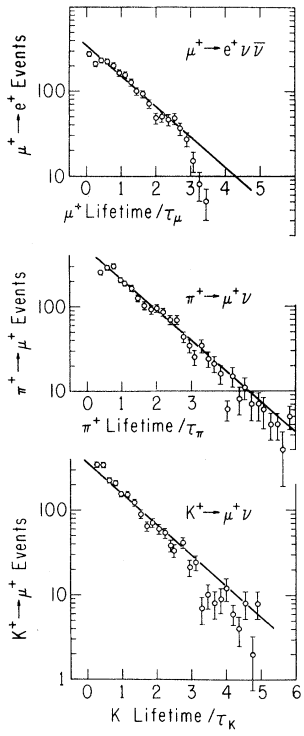

FIG. 12. Lifetime distributions: (a) $\mu^+ \to e^+ \nu \bar{\nu}$, (b) $\pi^+ \to \mu^+ \nu$, (c) $K^+ \to \mu^+ \nu$. The straight lines are the expected decay curves $e^{-t/\tau}$, where in each case τ is the accepted mean life. Some loss of μ's is expected near the ends of the traces due to poor focusing. The loss of short-lived π's is due to events in which the π^+ and μ^+ pulse were not separately observable. The calculated K^+ lifetime is sensitive to the calibration of the kaon time digitizer.

with energies corresponding to those from $K^+ \to \mu^+ \nu \gamma$ (mean γ energy > 90 MeV for events in which the μ^+ was within our range of sensitivity) was determined in a separate test. Pb-glass block B3 was replaced with a smaller block, B3′ (dashed line, Fig. 5), which was optically isolated and separated from the carbon stopper and from adjacent counters by $\frac{1}{4}$ in. lead plates. A record was made of $K^+ \to \pi^+ \pi^0$ events in which the stopping π^+ was accompanied by a large γ pulse (> 200 MeV) in B3′. Among 310 such events there were four in which no signal was observed from the other π^0 γ ray. Since the minimum angle (67°) between the π^0 γ's was larger than the maximum angle subtended by B3′ block (36°) and since the kinematics and the minimum B3′ pulse size ensured that the second γ had an energy < 50 MeV we concluded that the inefficiency for single γ's with energy 20–50 MeV was $I_\gamma \simeq 0.013$. This single γ inefficiency depended on the angular distribution of the γ's, hence it could not be used to make a reliable $K^+ \to \mu^+ \nu \gamma$ background calculation.

E. Calibrations

1. K^+, π^+, and μ^+ Lifetimes

The particle lifetime measurements did not enter directly into the calculation of the results. They were useful, however, in making internal checks of the detection system.

The K^+ lifetime was determined by the delay between the pulses from K3 and T1. The delay was digitized [with a time-to-amplitude converter–analog-to-digital converter (TAC-ADC) system] and displayed with counter lights as shown in Fig. 11. K decays of various lifetimes were simulated using scattered beam pions and inserting known lengths of signal cable into the T1 signal line.

The π^+ and μ^+ lifetimes were measured using the π-μ and μ-e pulse displacements on the oscilloscopes, where the sweep speeds were calibrated with series of timing pulses of known separation.

Using events up to 2.5 mean lives we obtain the values $\tau_K = 11.8 \pm 0.7$ ns, $\tau_\pi = 27.4 \pm 1.2$ ns, and $\tau_\mu = 2.15 \pm 0.10$ μs in satisfactory agreement with the accepted values 12.37 ns, 26.02 ns, and 2.20 μs, respectively.[12]

2. Comparison of Known Branching Ratios

A comparison of the known branching ratios $\Gamma(K^+ \to \pi^+ \pi^0)/\Gamma(K^+ \to \mu^+ \nu)$ and $\Gamma(K^+ \to \mu^+ \pi^0 \nu)/\Gamma(K^+ \to \mu^+ \nu)$ gave us an over-all check of our technique and a check on our calculations of pion transmission.

We used the relationships

$$\frac{\Gamma(K^+ \to \pi^+ \pi^0)}{\Gamma(K^+ \to \mu^+ \nu)} = \frac{\pi^+ \pi^0/K(\mathrm{III})}{\mu^+ \nu/K(\mathrm{IV})} \frac{\epsilon_{\mu^+ \nu}(\mathrm{IV})}{\epsilon_{\pi^+ \pi^0}(\mathrm{III})} \frac{1}{T(\mathrm{III}) C_\pi}$$

and

$$\frac{\Gamma(K^+ \to \mu^+ \pi^0 \nu)}{\Gamma(K^+ \to \mu^+ \nu)} = \frac{\mu^+ \pi^0 \nu/K(\mathrm{I})}{\mu^+ \nu/K(\mathrm{IV})} \frac{\epsilon_{\mu^+ \nu}(\mathrm{IV})}{\epsilon_{\mu^+ \pi^0 \nu}(\mathrm{I})}$$

to calculate these ratios, where $\pi^+ \pi^0/K(\mathrm{III})$ is the number of $\pi^+ \pi^0$ events divided by the corresponding number of stopping K^+ signals with degrader III; $\mu^+ \nu/K(\mathrm{IV})$ is the corresponding ratio for $\mu^+ \nu$ events with degrader IV; and $\mu^+ \pi^0 \nu/K(\mathrm{I})$ is the corresponding ratio for $\mu^+ \pi^0 \nu$ events with degrader I. Not all the "μ events" (degrader I) came from $K^+ \to \mu^+ \pi^0 \nu$ decays; some came from decay-in-flight of π^+ in $K^+ \to \pi^+ \pi^0$, $K^+ \to \pi^+ \pi^+ \pi^-$, and $K^+ \to \pi^+ \pi^0 \pi^0$ decays, some from $K^+ \to \mu^+ \nu \gamma$ decay, and some from unresolved π events. The real $\mu^+ \pi^0 \nu$ events were related to the observed μ and π events by

$$\mu^+ \pi^0 \nu \text{ events} = P_\mu \left[(\mu \text{ events}) - \left(\frac{1}{C_\pi} - 1 \right) (\pi \text{ events}) \right],$$

where P_μ is the fraction of μ events from $K^+ \to \mu^+ \pi^0 \nu$ decay. P_μ was calculated from the known geometry of the apparatus. For degrader I we obtained $P_\mu = 0.92$.

Using the values $\mu^+ \nu/K(\mathrm{IV}) = 1.19 \times 10^{-2}$, $\pi^+ \pi^0/K(\mathrm{III}) = 1.87 \times 10^{-3}$, $\mu^+ \pi^0 \nu/K(\mathrm{I}) = 1.92 \times 10^{-4}$ (no lifetime cuts were applied to these ratios), $T(\mathrm{III}) = 0.70$, $C_\pi = 0.66$, and the corresponding effective detection efficiencies (see Table III), we obtain

$$\frac{\Gamma(K^+ \to \pi^+ \pi^0)}{\Gamma(K^+ \to \mu^+ \nu)} = 0.32 \pm 0.02$$

and

$$\frac{\Gamma(K^+ \to \mu^+ \pi^0 \nu)}{\Gamma(K^+ \to \mu^+ \nu)} = 0.051 \pm 0.003$$

in satisfactory agreement with the accepted values[12] $(0.2092/0.6377) = 0.328$ and $(0.032/0.6377) = 0.050$.

F. Background

Since no background subtraction was made in either the $K^+ \to \mu^+ \nu \bar{\nu} \nu$ or the $K^+ \to \pi^+ \nu \bar{\nu}$ experiment—in the latter no events were seen—our estimates of the background do not enter into the calculation of the results. We shall therefore limit our discussion to a brief account of potential background sources indicating the likely origin of the unidentified μ events and the μ^+ and π^+ sources which may limit more sensitive experiments.

1. $K^+ \to \mu^+ \nu \gamma$

The radiative decay $K^+ \to \mu^+ \nu \gamma$ was the most serious source of background muons. The branching ratio of this decay is about 5.5×10^{-4} in the energy interval of the experiment (60 to 100 MeV). The γ is emitted preferentially along the direction of the muon, hence it may be converted in the degrader and evade detection. The water Čerenkov radiator TC and the pulse height criterion on the T3 counter served to reject events in which γ's were converted in the degrader. If we assume the measured single γ inefficiency $I_\gamma = 0.013$ for $K^+ \to \mu^+ \nu \gamma$ events which were not rejected by T3, we estimate that 13.3 such events would have been misidentified as "μ^+-no γ" events. Because of the uncertainties in the I_γ measurement we regard the close agreement of the calculated (13.3) and observed (14) numbers of "μ^+-no γ" events to be fortuitous. We believe that $K^+ \to \mu^+ \nu \gamma$ is the most likely source of the observed events in the $K^+ \to \mu^+ \nu \bar{\nu} \nu$ experiment.

2. K^+ Charge Exchange $\Rightarrow K_L^0 \to \mu^- \pi^+ \nu$

K^+ charge exchange in the carbon stopper followed by K_L^0 decay could produce $\mu(\pi)$ and simulate $\mu^+ \nu \bar{\nu} \nu$ ($\pi^+ \nu \bar{\nu}$) provided that the accompanying π (μ) remained within the stopper and hence escaped escaped detection. Because of the time delay requirement on K^+-decay signals (T1 pulse >3.3 ns

later than K3 pulse), only very low-energy K^0's would remain inside the stopper long enough for the μ (π) to be accepted.

We estimated the background due to this process using a linear extrapolation of the measured K^+-d charge-exchange cross section[13] and assuming that the carbon nucleus is the equivalent of six free deuterons. The estimated number of "$\mu^+\nu\bar{\nu}\nu$" ("$\pi^+\nu\bar{\nu}$") events due to charge exchange was <0.2 (<0.13).

3. $K^+\to\mu^+\pi^0\nu$

Muons from $K^+\to\mu^+\pi^0\nu$ would fall in the same range interval as those from $K^+\to\mu^+\nu\bar{\nu}\nu$. With a π^0 inefficiency $I_{\pi^0}<2.2\times10^{-5}$ the expected rate at which this could simulate "$\mu^+\nu\bar{\nu}\nu$" events was less than 2.7×10^{-7}. Hence, this source of background could be neglected.

4. *Scattered Beam Pions*

Scattered beam pions could, in principle, produce background π's and μ's. With the time-delay requirement removed between K3 and T1, scattered pions were observed at the rate of 2 per 10^6 stopping K^+. In order for these to be mistaken for $K^+\to\mu^+(\pi^+)+$neutrals, one would have to miss all the K^+ decay products. Using the normal delay requirement we estimate a background $\ll10^{-3}$.

5. $K^+\to\pi^+\pi^-\mu^+\nu$, $\pi^+\pi^-e^+\nu$

We estimated the background contribution from $K^+\to\pi^+\pi^-\mu^+\nu$ decays by assuming the μ spectrum to be similar to the well-studied e spectrum from $K^+\to\pi^+\pi^-e^+\nu$.[14] Using the Pais-Treiman differential-decay distribution,[15] we estimate that only about 6×10^{-4} (3×10^{-4}) of the μ (π) spectrum had a range that could reach the decay counters. Considering the known (1×10^{-5}) branching ratio for this decay mode, the effective rate for this decay was clearly negligible.

The $K^+\to\pi^+\pi^-e^+\nu$ decay gave a much larger fraction ($\frac{1}{4}$) of the π^+ spectrum above our minimum detectable energy. But from our estimate of the probability that the π^- and e^+ would both escape detection and from the known branching ratio (3.3×10^{-5}), we calculate a "$\pi^+\nu\bar{\nu}$" background of <0.04 events due to this process.

V. RESULTS

A. Final Sample

We found fourteen events which satisfied the triggering logic, range requirement, and scanning criteria for $K^+\to\mu^+\nu\bar{\nu}\nu$. To these, as to all $K^+\to\mu^+\nu$ and $K^+\to\mu^+\pi^0\nu$ events, we applied cuts on lifetime ($t_K<2.5\ \tau_K$, $t_\mu<2.5\ \tau_\mu$) and on T3 pulse height (see Fig. 13). We thus obtained a sample of ten "$\mu^+\nu\bar{\nu}\nu$" events.

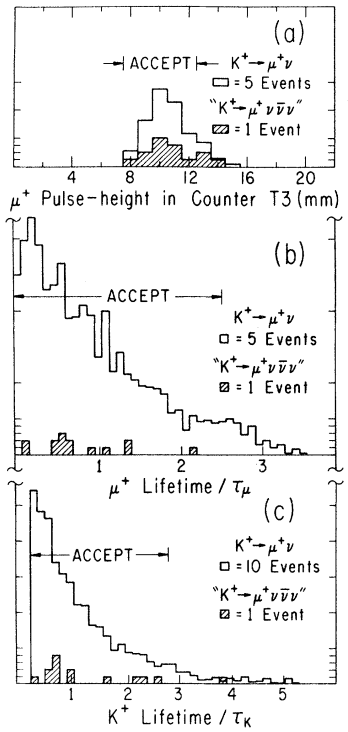

FIG. 13. Characteristics of $K^+\to\mu^+\nu\bar{\nu}\nu$ sample events (shaded histograms) compared with those of $K^+\to\mu^+\nu$ events (open histograms). (a) Muon pulse-height distributions in T3 counter. (b) Muon lifetime distributions. (c) Kaon lifetime distributions.

We could, in principle, subtract the estimated 13.3-event background due to misidentified $\mu^+\nu\gamma$ events, but because of the uncertainties in estimating the background we do not feel justified in making such a subtraction. We prefer to calculate limits on $K^+\to\mu^+\nu\bar{\nu}\nu$ based on a sample of ten unidentified events.

Since we wish to present 90% confidence limits, we shall compute our results using a "true" event rate (15.4 events) such that in 90% of such experiments one would expect to find more than 10 events (assuming a Poisson distribution).

B. Limit on the $K^+\to\mu^+\nu\bar{\nu}\nu$ Decay Rate

1. *Partial Decay Rate; $60<T_\mu<100$ MeV*

For the interval we have examined, 16–34 g/cm^2 in carbon ($60<T_\mu<100$ MeV), we may calculate a partial decay rate which is nearly independent of the assumed μ^+ spectrum. We use the expression

$$\frac{\Gamma(K^+\to\mu^+\nu\bar{\nu}\nu;\ 60<T_\mu<100\ \text{MeV})}{\Gamma(K^+\to\mu^+\nu)}$$

$$=\frac{\mu^+\nu\bar{\nu}\nu}{E(\text{I})K(\text{I})+E(\text{II})K(\text{II})}\ \frac{\epsilon_{\mu+\nu}(\text{IV})K(\text{IV})}{\mu^+\nu}\ R\ ,$$

TABLE IV. Effective detection efficiency for degraders I and II and resultant upper limit on the $K^+ \to \mu^+ \nu\bar{\nu}\nu$ decay rate (90% confidence level) for assumed spectra.

Type of first order interaction	$\epsilon_{\mu^+\nu\bar{\nu}\nu}$(I)	$\epsilon_{\mu^+\nu\bar{\nu}\nu}$(II)	$\frac{\Gamma(K^+ \to \mu^+ \nu\bar{\nu}\nu)}{\Gamma(K^+ \to \mu^+ \nu)}$	$\frac{\Gamma(K^+ \to \mu^+ \nu\bar{\nu}\nu)}{\Gamma(K^+ \to \text{all})}$
neutrino-neutrino [a]	4.47×10^{-3}	3.36×10^{-3}	$<9.4\times10^{-6}$	$<6.0\times10^{-6}$
six-fermion [b]	3.99×10^{-3}	3.06×10^{-3}	$<10.5\times10^{-6}$	$<6.7\times10^{-6}$

[a] Reference 3.
[b] Reference 5.

where $\mu^+\nu\bar{\nu}\nu$ = "true" number of unidentified events (15.4), $E(\text{I}) = 0.0089$ and $E(\text{II}) = 0.0120$ are the average geometric detection efficiencies over the observed range interval with degrader I and II, $K(\text{I}) = 5.8\times10^8$ and $K(\text{II}) = 4.44\times10^8$ are the numbers of stopping K's with degraders I and II, $\epsilon_{\mu^+\nu}(\text{IV}) = 0.018\,43$ is the overlap of the geometric efficiency for degrader IV with the μ^+ range spectrum for $\mu^+\nu$ decays, $\mu^+\nu/K(\text{IV}) = 1.14\times10^{-2}$, and $R = 1.48$. With the values given, we obtain the partial rate

$$\frac{\Gamma(K^+ \to \mu^+ \nu\bar{\nu}\nu;\ 60 < T_\mu < 100\ \text{MeV})}{\Gamma(K^+ \to \mu^+ \nu)} \leq 3.5\times10^{-6}$$

or

$$\frac{\Gamma(K^+ \to \mu^+ \nu\bar{\nu}\nu;\ 60 < T_\mu < 100\ \text{MeV})}{\Gamma(K^+ \to \text{all})} \leq 2.2\times10^{-6}\ .$$

2. *Total Decay Rate*

Our limit on the total decay rate depends on the assumed shape of the muon spectrum. We use the expression

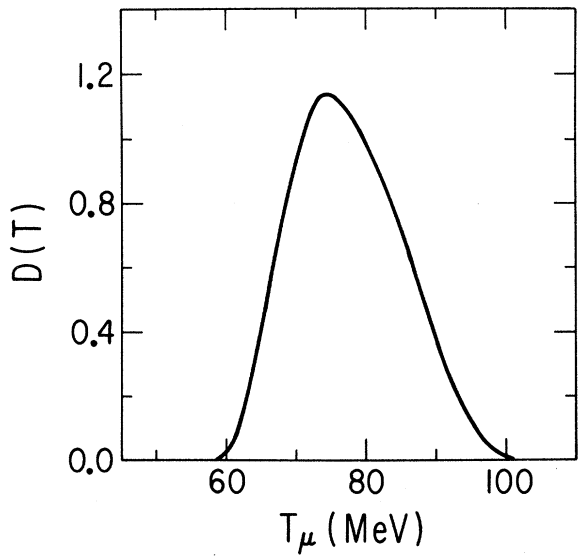

FIG. 14. Prescription curve for obtaining the differential detector efficiency for any assumed spectrum of $K^+ \to \mu^+\nu\bar{\nu}\nu$. The function $D(T)$ is discussed in Sec. V B3.

$$\frac{\Gamma(K^+ \to \mu^+ \nu\bar{\nu}\nu)}{\Gamma(K^+ \to \mu^+ \nu)} = \frac{\mu^+\nu\bar{\nu}\nu}{\epsilon_{\mu^+\nu\bar{\nu}\nu}(\text{I})K(\text{I}) + \epsilon_{\mu^+\nu\bar{\nu}\nu}(\text{II})K(\text{II})} \times \frac{\epsilon_{\mu^+\nu}(\text{IV})K(\text{IV})}{\mu^+\nu} R\ ,$$

where the various terms have the same values as above except $\epsilon_{\mu^+\nu\bar{\nu}\nu}$(I) and $\epsilon_{\mu^+\nu\bar{\nu}\nu}$(II), which are the overlaps of the geometric efficiencies for degraders I and II with the assumed μ^+ spectrum. In Table IV we show the values of $\epsilon_{\mu^+\nu\bar{\nu}\nu}$ and the corresponding results for the spectra discussed in Sec. II B.

The most general statement of our results is that given in Sec. V B 3.

3. *Prescription for Branching Ratio Corresponding to Any Assumed Spectrum*

The limit on the branching ratio corresponding to any assumed spectrum may be calculated from our data by the following procedure:

(i) Normalize the assumed μ^+ spectrum $F(T)$ such that

$$\int F(T)dT = 1\ .$$

(ii) Compute the overlap

$$\int D(T)F(T)dT\ ,$$

using the function $D(T)$ as given in Fig. 14. This function is normalized in such a way that

$$\int D(T)F(T)dT = \frac{\epsilon_{\mu^+\nu\bar{\nu}\nu}}{\epsilon_{\mu^+\nu}}$$

[i.e., $D(T)$ = Ratio of geometrical efficiency with degraders I and II to effective efficiency for $K^+ \to \mu^+\nu$ with degrader IV.]

(iii) Find the branching ratio using the expression

$$\frac{\Gamma(K^+ \to \mu^+ \nu\bar{\nu}\nu)}{\Gamma(K^+ \to \mu^+ \nu)} = \frac{\mu^+\nu\bar{\nu}\nu/K(\text{I+II})}{\mu^+\nu/K(\text{IV})} \frac{\epsilon_{\mu^+\nu}}{\epsilon_{\mu^+\nu\bar{\nu}\nu}} R\ .$$

Inserting the numerical values which have been given, this expression becomes

$$\frac{\Gamma(K^+\to\mu^+\nu\bar{\nu}\nu)}{\Gamma(K^+\to\mu^+\nu)}<\frac{2.0\times10^{-6}}{\int D(T)F(T)dT}$$

(90% confidence level)

or

$$\frac{\Gamma(K^+\to\mu^+\nu\bar{\nu}\nu)}{\Gamma(K^+\to\text{all})}<\frac{1.3\times10^{-6}}{\int D(T)F(T)dT}$$

(90% confidence level).

ACKNOWLEDGMENTS

We are grateful to Professor E. Segrè for his encouragement and support and to Gary Lum and Harlan Evans for assistance during portions of the experiment. We thank the operating crew of the Bevatron for their cooperation. We are also thankful to Professor M. Kislinger for helpful discussions and to J. Curry and J. Klems for reading the manuscript.

APPENDIX: CALCULATION OF THE $K^+\to\mu^+\nu\bar{\nu}\nu$ DECAY RATE IN CONVENTIONAL THEORY

In evaluating the rate for the $K^+\to\mu^+\nu\bar{\nu}\nu$ decay, we consider here only the lowest-order diagrams which are allowed in the framework of current-current theory of weak interactions (see Fig. 1).

The differential-decay rate is calculated by the expression

$$d\Gamma=\int\sum_{\text{spin}}|T|^2(2\pi)^4\delta^4(k-p-p_1-p_2-p_3)\times d^3p\,d^3p_1d^3p_2d^3p_3\,, \tag{A1}$$

where k, p, and p_i $(i=1,2,3)$ are the four-momentum of the kaon, muon, and neutrinos, and T is the transition matrix element,

$$T=\left(\frac{G}{\sqrt{2}}\right)^2\frac{1}{(2\pi)^6}\left(\frac{1}{2E_\mu}\frac{1}{2E_1}\frac{1}{2E_2}\frac{1}{2E_3}\right)^{1/2}\langle0|A_\lambda|K\rangle\times\left[\bar{\nu}_3\gamma_\lambda(1+\gamma_5)\frac{1}{\not{p}_l-m_l}\gamma_\delta(1+\gamma_5)\nu_1\right]\times[\bar{\mu}\gamma_\delta(1+\gamma_5)\nu_2]\,,$$

in which $\langle0|A_\lambda|K\rangle$ is the strangeness-changing axial-vector-current matrix element

$$\langle0|A_\lambda|K\rangle=\frac{f_K}{(2E_K)^{1/2}}k_\lambda\,,$$

with p_l and m_l the four-momentum and mass of the virtual lepton ($l=\mu$ or e) in the intermediate state, and $|f_K|=0.25\,m_\pi$ is the K-decay constant. We use the units $\hbar=c=1$ and the metric $g_{\mu\nu}=(-1,-1,-1,1)$.

Let

$$B_{\lambda\delta}=\bar{\nu}_3\gamma_\lambda(1+\gamma_5)\frac{1}{\not{p}_l-m_l}\gamma_\delta(1+\gamma_5)\nu_1\,.$$

Using the relations of four-momentum and the properties of γ matrices, this becomes

$$B_{\lambda\delta}=\frac{2}{m_K{}^2-2m_KE_3-m_l{}^2}\bar{\nu}_3\gamma_\lambda\gamma\cdot(k-p_3)\gamma_\delta(1+\gamma_5)\nu_1.$$

Therefore,

$$k_\lambda B_{\lambda\delta}=\frac{2(m_K{}^2-2m_KE_3)}{m_K{}^2-2m_KE_3-m_l{}^2}\bar{\nu}_3\gamma_\delta(1+\gamma_5)\nu_1\,.$$

Squaring T and summing over the spins in the final state, we have

$$\begin{aligned}\sum_{\text{spin}}|T|^2&=\frac{G^4}{4}\frac{1}{(2\pi)^{12}}\frac{f_K{}^2}{2m_K}\frac{4m_K{}^2(m_K-2E_3)^2}{(m_K{}^2-2m_KE_3-m_l{}^2)^2}\\&\times\frac{1}{2E_\mu2E_12E_22E_3}\,\mathrm{Tr}\,[\gamma_\delta(1+\gamma_5)\not{p}_3\gamma_\lambda(1+\gamma_5)\not{p}_1]\\&\times\mathrm{Tr}\,[(\not{p}+m_\mu)\gamma_\delta(1+\gamma_5)\not{p}_2\gamma_\lambda(1+\gamma_5)]\\&=\frac{128G^4f_K{}^2}{(2\pi)^{12}}\frac{m_K(m_K-2E_3)^2}{(m_K{}^2-2m_KE_3-m_l{}^2)^2}\\&\times\frac{1}{2E_\mu2E_12E_22E_3}\,p_1\cdot p\,p_2\cdot p_3\,.\end{aligned}\tag{A2}$$

Substituting Eq. (A2) into Eq. (A1) and integrating over p_1, p_2, and p_3 with the use of Lenard's formula

$$\int k_1^\alpha k_2^\beta\delta^4(k-k_1-k_2)\frac{d^3k_1}{2E_1}\frac{d^3k_2}{2E_2}=\frac{1}{24}\pi[2k^\alpha k^\beta+g^{\alpha\beta}(k\cdot k)]\,,$$

we obtain the following expression for the energy spectrum of the decay muon:

$$\begin{aligned}\frac{d\Gamma}{dE_\mu}=\frac{8G^4f_K{}^2}{9(2\pi)^5m_K}&\{[4A(E_\mu)-3m_KB(E_\mu)](4E_\mu{}^2-3m_KE_\mu)\\&-2m_\mu{}^2[2A(E_\mu)+3m_KB(E_\mu)]\}\\&\times(E_\mu{}^2-m_\mu{}^2)^{1/2}\,.\end{aligned}\tag{A3}$$

The functions $A(E_\mu)$ and $B(E_\mu)$ are given by the integrals

$$A(E_\mu)=\int_0^{E_3^{\max}}\frac{(\frac{1}{2}m_K-E_3)^2E_3{}^3dE_3}{[E_3-(m_K{}^2-m_l{}^2)/2m_K]^2}\,,$$

$$B(E_\mu)=\int_0^{E_3^{\max}}\frac{(\frac{1}{2}m_K-E_3)^2E_3{}^2dE_3}{[E_3-(m_K{}^2-m_l{}^2)/2m_K]^2}\,,$$

with $E_3^{\max}=\frac{1}{2}(m_K+p_\mu-E_\mu)$, the maximum energy of the neutrino corresponding to the momentum p_μ and total energy E_μ of the muon. Comparing Eq. (A3) to the $K^+\to\mu^+\nu$ decay rate, we obtain

$$\frac{(d\Gamma/dE_\mu)(K^+ \to \mu^+ \nu \bar{\nu} \nu)}{\Gamma(K^+ \to \mu^+ \nu)} = \frac{2G^2}{9\pi^4 m_\mu{}^2 m_K{}^2}\left(1-\frac{m_\mu{}^2}{m_K{}^2}\right)^{-2} \{[4A(E_\mu) - 3m_K B(E_\mu)](4E_\mu{}^2 - 3m_K E_\mu) - 2m_\mu{}^2[2A(E_\mu) + 3m_K B(E_\mu)]\}(E_\mu{}^2 - m_\mu{}^2)^{1/2} .$$

The partial decay rate in the muon kinetic energy interval 60–100 MeV is obtained by integrating Eq. (A3) over this energy interval. For the case of $l = e$ the rate is

$$\frac{\Gamma(K^+ \to \mu^+ \nu_e \bar{\nu}_e \nu_\mu;\ 60 < T_\mu < 100\ \text{MeV})}{\Gamma(K^+ \to \mu^+ \nu)} = 2.0 \times 10^{-16} .$$

For the case of $l = \mu$, the decay rate is half of that given by Eq. (A3), because there are two identical neutrinos in the final state. This gives

$$\frac{\Gamma(K^+ \to \mu^+ \nu_\mu \bar{\nu}_\mu \nu_\mu;\ 60 < T_\mu < 100\ \text{MeV})}{\Gamma(K^+ \to \mu^+ \nu)} = 1.7 \times 10^{-16}.$$

The decay rate for the process $K^+ \to \mu^+ \nu \bar{\nu} \nu$ is the sum of these two distinct processes, which gives

$$\frac{\Gamma(K^+ \to \mu^+ \nu \bar{\nu} \nu;\ 60 < T_\mu < 100\ \text{MeV})}{\Gamma(K^+ \to \mu^+ \nu)} = 3.7 \times 10^{-16} .$$

*Research supported by the U. S. Atomic Energy Commission and by the National Science Foundation under Grant No. 29717.

†Thesis submitted by C. Y. Pang to the Department of Physics, the University of Chicago, in partial fulfillment of the requirements for the Ph.D. degree.

‡Now at the National Accelerator Laboratory, Batavia, Illinois 60510.

[1]G. D. Cable, R. H. Hildebrand, C. Y. Pang, and R. Stiening, Phys. Lett. 40B, 669 (1972).

[2]M. Gell-Mann, M. L. Goldberger, N. M. Kroll, and F. E. Low, Phys. Rev. 179, 1518 (1969).

[3]D. Yu. Bardin, S. M. Bilenky, and B. Pontecorvo, Phys. Lett. 32B, 121 (1970); B. Pontecorvo, Joint Institute for Nuclear Research, Dubna, Report No. E1-5439 (unpublished); D. Yu. Bardin and S. M. Bilenky, Joint Institute for Nuclear Research, Dubna, Report No. E2-5881 (unpublished).

[4]T. Ericson and S. L. Glashow, Phys. Rev. 133, B130 (1964).

[5]A. Vanzha, A. Isaev, and L. Lapidus, Yad. Fiz. 12, 595 (1970) [Sov. J. Nucl. Phys. 12, 325 (1971)].

[6]Z. Bialynicki-Birula, Nuovo Cimento 33, 1484 (1964).

[7]G. Danby, J. M. Gaillard, K. Goulianos, L. M. Lederman, N. Mistry, M. Schwartz, and J. Steinberger, Phys. Rev. Lett. 9, 36 (1962).

[8]We derive (3) from Eq. (49) of Ref. 5, using the relationship

$$\Gamma(K^+ \to \mu^+ \nu) = G^2 f_K^2 m_\mu{}^2 m_K [1 - (m_\mu/m_K)^2]^2/8\pi.$$

Our coefficient (0.3) differs from the value (1.9×10^{-2}) shown in Eq. (56) of Ref. 5.

[9]K. S. Heard, J. Heintze, G. Heinzelmann, P. Igo-Kemenes, W. Kalbreier, E. Mittag, H. Rieseberg, B. Schürlein, H. W. Siebert, V. Soergel, K. P. Streit, A. Wagner, and A. H. Walenta, paper contributed to the XVI International Conference on High Energy Physics, Chicago-Batavia, Ill., 1972 (unpublished).

[10]K. Borer, B. Hahn, H. Hofer, H. Kaspar, F. Krienen, and P. Seiler, Phys. Lett. 29B, 164 (1969).

[11]H. W. Bertini, Phys. Rev. 131, 1801 (1963); Phys. Rev. 138, AB2 (1965).

[12]Particle Data Group, Phys. Lett. 39B, 1 (1972).

[13]W. Slater, D. H. Stork, H. K. Ticho, W. Lee, W. Chinowsky, G. Goldhaber, S. Goldhaber, and T. O'Halloran, Phys. Rev. Lett. 7, 378 (1961).

[14]M. Bourquin, J. P. Boymond, P. Extermann, J. Marasco, R. Mermod, P. A. Piroué, H. Suter, P. Basile, S. Brehin, A. Diamant-Berger, P. Kunz, M. Lemoine, R. Turlay, and A. Zylbersztejn, Phys. Lett. 36B, 615 (1971); P. Basile *et al.*, *ibid.* 36B, 619 (1971).

[15]A. Pais and S. B. Treiman, Phys. Rev. 168, 1858 (1968)

[16]N. Cabibbo, Nuovo Cimento 11, 837 (1959).

[17]R. J. Abrams, A. S. Carroll, T. F. Kycia, K. K. Li, J. Menes, D. N. Michael, P. M. Mockett, and R. Rubinstein, Phys. Rev. Lett. 29, 1118 (1972).